Adsorption (2013) 19:745–756
DOI 10.1007/s10450-013-9507-6

Effect of surface functionalities on gas adsorption in microporous carbons: a grand canonical Monte Carlo study

A. Gotzias · E. Tylianakis · G. Froudakis · Th. Steriotis

Received: 31 October 2012 / Accepted: 5 February 2013 / Published online: 14 February 2013

Abstract In an attempt to offer a more realistic picture of adsorption in highly heterogeneous porous systems, such as oxygen functionalized porous carbons, we consider a series of carbon surfaces baring different amounts of oxygen functionalities (hydroxyl and epoxy). These surfaces are used to construct "oxidized" slit pores of varying width and functionality. With the aid of such inhomogeneous structures we study the interaction of Ar (87 K) inside "functionalized" pores and report grand canonical Monte Carlo adsorption simulations results. Based on our simulation data, we discuss the role of chemical heterogeneity on adsorbed/gas phase equilibrium properties such as density, heat of adsorption, and molecular packing within the pores. Comparisons are made with the case of the oxygen–free (completely homogeneous) slit pore models and conclusions on the suitability of Ar based pore size distributions for functionalized porous carbons are drawn.

Keywords Argon adsorption · Oxidized carbon · Heterogeneity · Confinement · Monte Carlo simulation

1 Introduction

Porous carbons are solids with a highly developed pore structure containing mainly micropores although meso and macropores can also be present depending on the carbon precursor and the synthesis procedure applied (Marsh and Rodriguez-Reinoso 2006). Numerous experimental studies provide indications that carbon based systems usually include both aromatic and aliphatic structures as well as a variety of surface functional groups, the majority of which contain oxygen (e.g., hydroxyl, epoxy, carboxyl, carbonyl) (Haenel 1992; Smith et al. 1994; van Krevelen 1991; White et al. 2005). The oxygen content on carbon surfaces can up to a certain degree be controlled by using simple oxidative agents, during chemical treatment or activation (Lee and Park 2012; Wang et al. 2010). Pyrolysis produced carbon are characterized by a mixture of amorphous and graphitic nanosized domains that give rise to a "card stack" pore system usually simulated with slit geometries. Functional groups are mainly introduced at edge carbons e.g., at the boundaries of graphene sheets of the graphitic nanodomains but also all over their surfaces were defects have been developed (e.g., during pyrolysis or activation). A more "heavily" oxygen functionalized case of carbonaceous materials is that of porous graphene oxides where oxygen groups exist mainly as active sites on the basal surface. In this respect it is important both from a practical and a fundamental perspective to examine the influence of

This work was originally presented in ISSHAC 8.

A. Gotzias (✉) · Th. Steriotis
Institute of Advanced Materials, Physicochemical Processes, Nanotechnology and Microsystems, NCSR Demokritos, Agia Paraskevi, 15310 Athens, Greece
e-mail: agotzias@chem.demokritos.gr

E. Tylianakis
Department of Materials Science and Technology, University of Crete, 71409 Heraklion, Crete, Greece

Present Address:
E. Tylianakis
Department of Chemical and Biological Engineering, Northwestern University, 2145 Sheridan Road, Evanston, IL 60208, USA

G. Froudakis
Department of Chemistry, University of Crete, Voutes, 71003 Heraklion, Crete, Greece

oxygen functionalization of carbon pores on the material adsorption behavior.

Despite the fact that oxidized graphitic structures (and also graphene oxides, GO) have been known for a long time, few statistical molecular simulations of gas adsorption have explicitly taken pore surface oxygen content into account. Tenney and Lastoskie (2006) carried out molecular simulations in graphitic models with hydroxyl and carboxyl groups, Liu and Wilcox (2012) estimated CO_2 adsorption in combined hydroxyl–carbonyl functionalized carbon surfaces, Gotzias et al. (2012) studied hydrogen adsorption in oxygen functionalized slit pores. In general the existence of oxygen groups has been considered as an element of surface heterogeneity having statistically the same or similar effect with surface irregularities, defects, etc. In this respect, Puibasset (2005) compared the adsorption of argon in geometrically and chemically undulated models of cylindrical pores by introducing parameters of surface roughness on solid fluid potentials based upon a mean field interaction model of cylinders (Tjatjopoulos et al. 1998). Wang et al. (2011) based on a similar model studied the adsorption of argon in cylindrical pores by introducing patches of different surface strength to account for the presence of oxygen atoms. Although this approach is simpler than other models proposed in the literature (Coasne et al. 2006; Pellenq and Levitz 2002; Kuchta et al. 2007; Palmer and Gubbins 2012; Monson 2012) it has been found that by including surface heterogeneity in modeling adsorption systems, one can successfully describe experimental isotherms in the low pressure or coverage range where solid–fluid (s–f) interactions prevail (Rowley et al. 1976; Maddox et al. 1997).

For this reason Neimark et al. (2009) presented a new model of adsorption in micro–mesoporous carbons based on the quenched solid density functional theory (QSDFT), which in contrast to the non local DFT (NLDFT) that predates this, accounts for surface heterogeneity in terms of a roughness parameter. QSDFT has been widely used (Miyasaka et al. 2009; Silvestre-Albero et al. 2012; Liu and Wilcox 2012; Gor et al. 2012) for a series of diverse carbon structures. In the same context several approaches to introduce elements of heterogeneity into molecular simulations have been developed and used (Jagiello and Olivier 2009; Bhatia 2002; Ravikovitch et al. 2001; Wisniewski et al. 2012). In most of the cases the modeling results have been compared with real materials, which however are not well defined at least in terms of surface oxygen content. Furmaniak et al. (2009) has studied the influence of the type of adsorbate on the pore size distribution, by varying the oxygen content on a virtual porous carbon model. Argon as a probe can reproduce postulated pore size distributions regardless the surface oxygen content, while other probe molecules as N_2 or CO_2 cannot due to induced dipole moments stemming from adsorbate–oxygen interactions. Our intention is to consider individual pore models with atomistically defined graphitic surfaces baring oxygen functional groups and a rigorous statistical model such as grand canonical Monte Carlo (GCMC) to describe the adsorption mechanism and the effect of surface heterogeneity to the adsorption capacity. This approach could in principle function as a "benchmark" on which more general heterogeneity approaches can be applied and tested. It should be noted that in general, individual (slit or cylinder) pore models cannot capture the structure of real porous materials. Nevertheless, they are abundantly used (e.g., for deducing pore size distributions) since local equilibria (at the nanoscale) can be predicted and thus simulation of the equilibrium behavior of real porous materials is feasible.

In this paper, the results of a GCMC study of argon adsorption at 87 K are reported for explicit models of carbon pore surfaces that bare combined hydroxyl and epoxy groups. The oxygen content on the surface varies from very high to very low and the reported uptakes are compared to pores with homogeneous graphitic walls. The role of chemical heterogeneity in determining the adsorption capacity and adsorbed/gas phase equilibrium properties such as density, heat of adsorption, and packing within the pore is discussed.

2 Models and simulation approach

2.1 Surfaces, pores and potential models

Eight different oxygen containing functionalized surfaces have been considered. The surfaces are actually graphene sheets, on one side of which, epoxy and hydroxyl groups have been randomly grafted (Fig. 1a). Graphite oxide cluster structures were optimized for both hydroxyl and epoxy configurations. Optimizations were conducted with Turbomole software at the DFT level of theory using the B-P86 functional and the def2-TZVP basis sets for all atom types (Ahlrichs et al. 1989). The resolution-of-the-identity (RI) approximation was used in all calculations for computing the electronic Coulomb interaction. For the epoxy case, oxygen atoms bridge over two neighboring carbon atoms forming 1.44 Å long C–O bonds. The C–O bond length of hydroxyl groups is 1.47 Å and the oxygen atom lies on top of a carbon atom normal to the plane. The C–O–H bond angle is 107.9°. The oxygen content varied from very low (C:O = 30:1 or $C_{30}O$) to high (C:O = 6:1 or C_6O) and the functionalized graphene sheets have been energetically relaxed. Due to the carbon hybridization changes upon grafting (sp^2–sp^3) the functional groups create local surface geometric perturbations and thus the produced models are rather corrugated than planar honeycomb lattices. C_nO refers to the total

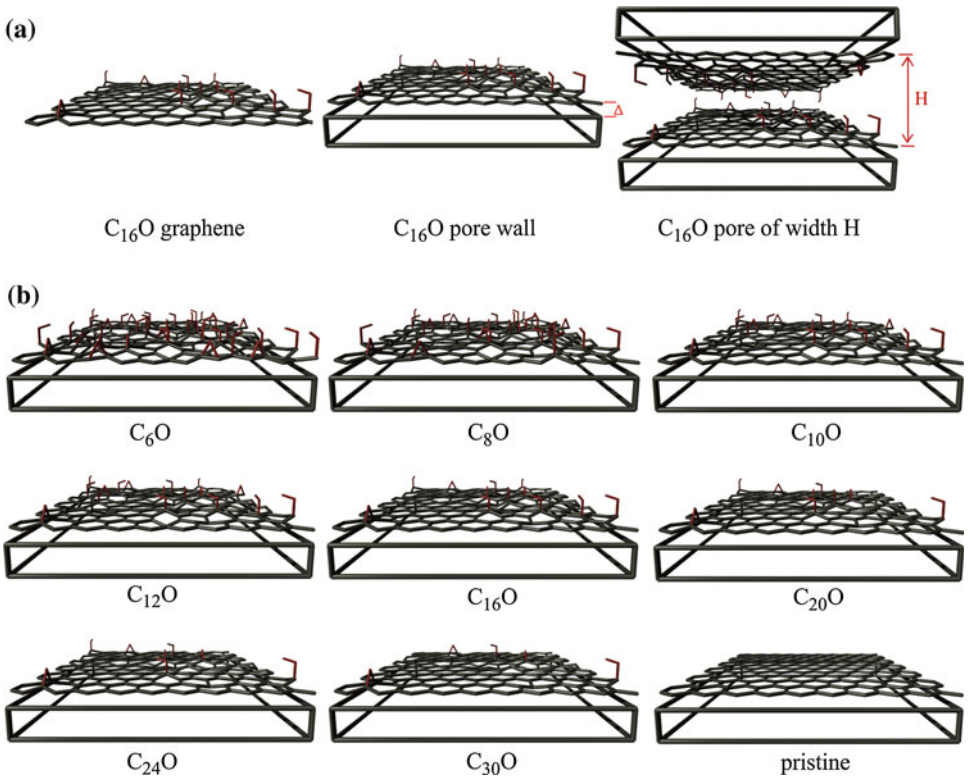

Fig. 1 **a** $C_{16}O$ graphene, pore wall comprising the $C_{16}O$ graphene over a mean field graphitic structure, an oxygen functionalized ($C_{16}O$) model slit pore and **b** all the considered pore walls with different content of oxygen functionalization

(hydroxyl and epoxy) oxygen content. For a given surface oxygen content, the hydroxyl to epoxy groups ratio is 2 (thus the correct molecular formula of our structures is $C_{3n}O_3H_2$, but we use the C_nO nomenclature for simplicity).

These one-side functionalized single-layer graphene sheets (closely resembling graphene oxides and/or partially reduced graphene oxides) were consequently considered to be on top (at a distance $\Delta = 0.335$ nm) of graphitic structures comprising an infinite number of stacked pure graphene layers, i.e., the functionalized graphene is the "wetted" part (of the otherwise graphitic structures) that can come in contact with fluids. Finally, these (multiwall) surface oxidized graphitic structures were used as walls to construct slit shaped pores of varying width, H. This was carried out by placing two identical (however inverted) walls at a distance H from each other (Fig. 1a). With this method 9 pores were constructed for each surface oxidation degree (including the pristine case). Their sizes range from H = 0.6 to H = 3.0 nm.

Based on the above, only the "wetted" (functionalized) graphene layer is described atomistically, while a mean-field approach was used for the "underlying" graphitic structure of the walls (Fig. 1b). For comparison with pristine (non-functionalized) graphitic walls, a single, atomistically described graphene layer (pure flat, hexagonal sp^2 hybridization) was also used on top of the underlying graphitic structure instead of its functionalized analogues. Additionally, for the sake of comparison with literature data, a full mean field approach was used to describe the pristine (non-functionalized) wall. In all cases, argon molecules were treated as one-site spherical particles. All atom–atom interactions were considered to be of Lennard-Jones type:

$$U_{ij}(r) = 4\varepsilon_{ij}\left(\left(\frac{\sigma_{ij}}{r}\right)^{12} - \left(\frac{\sigma_{ij}}{r}\right)^{6}\right) \quad (1)$$

where σ_{ij} and ε_{ij} are, respectively, the LJ size and energy parameters for the interaction of atom i with j, and r is the distance separating the two interacting particles. The potential model parameters used are listed in Table 1. The corresponding parameters for LJ interactions between different particles were deduced by Lorentz–Berthelot mixing rules.

Table 1 Potential model parameters used in GCMC simulations

Site	Lennard-Jones parameters		
	σ (nm)	ε/k (K)	Reference
Ar	0.3305	118.05	Neimark et al. (1998)
Surface atoms			
C (graphene)	0.340	28	Steele (1973)
O (O–H or C–O)	0.310	79	Tenney and Lastoskie (2006)
H (O–H)	0.130	30	

By following the approach described the interaction of an argon molecule, j, with the top layer of the wall is given by the sum $\sum_i U_{ij}(r_{ij})$, which runs over all (carbon, oxygen or hydrogen) atoms of the layer. The underlying graphene layers of the wall produce an additional mean field potential which is given by the (10-4-3) function of Steele (1974):

$$U(z)=2\pi\varepsilon_{jC}\rho_C\sigma_{jC}^2\Delta\left[\frac{2}{5}\left(\frac{\sigma_{jC}}{z}\right)^{10}-\left(\frac{\sigma_{jC}}{z}\right)^{4}-\frac{\sigma_{jC}^4}{3\Delta(z+0.61\Delta)^3}\right] \quad (2)$$

where, $\rho_C = 114\ \text{nm}^{-3}$ is the number density of carbon atoms, assuming that the length of the C–C bond is 0.142 nm, $\Delta = 0.335$ nm, is the separation between the graphene layers, and z is the distance between a fluid molecule and the mean field graphitic structure.

2.2 Grand canonical Monte Carlo simulations

Argon adsorption isotherms were computed by the grand canonical Monte Carlo method (Allen and Tildesley 1987). We used a simulation box, containing a slit pore, with periodic boundary conditions and minimum image convention in x and y directions (the pore width H is on the z direction). The lateral edges of the simulation box are (x, y) = (2.44, 2.34) nm. Volume, temperature and chemical potential were fixed, while in each Monte Carlo step a random displacement, creation or deletion of a single fluid molecule, was attempted with equal probabilities. The acceptance ratio for displacements was adjusted inside the range of (40–60 %) by properly modifying the maximum length of the molecules displacement vector. The grand canonical ensemble simulations utilized 25×10^6 configurations; the first 12.5×10^6 configurations were discarded to guarantee equilibration. All simulations were performed at 87 K. Each adsorption isotherm constitutes of 50 equilibration points in the range 1×10^{-7}–1 bar. The intervals between successive isotherm points increased with pressure exponentially. The GCMC based isosteric heats of adsorption have been calculated from the fluctuations of the number of particles and the total energy according to:

$$Q_{st} = RT - \frac{\langle UN\rangle - \langle U\rangle\langle N\rangle}{\langle N^2\rangle - \langle N\rangle^2} = \left[RT - \frac{\langle U_{ff}\rangle\langle N\rangle - \langle U_{ff}N\rangle}{\langle N^2\rangle - \langle N\rangle^2}\right] - \frac{\langle U_{sf}\rangle\langle N\rangle - \langle U_{sf}N\rangle}{\langle N^2\rangle - \langle N\rangle^2}. \quad (3)$$

where Q_{st} is the isosteric heat of adsorption per mol of argon, $T = 87$ K, R is the gas constant; $\langle\rangle$ is the ensemble average, N is the number of argon particles and U is the configuration energy of the system. The second equality of Eq. 3 shows two contributions to the isosteric heat: one is due to the fluid–fluid (f–f) and the other due to s–f interactions, that is, $U = U_{ff} + U_{sf}$.

The "physical" pore width, H, is defined as the distance between the planes passing through the centers of carbon atoms of the "inner" most (wetted) layers of the opposing walls (Fig. 1a). In reality, molecules cannot access the volume defined by H due to the space occupied by surface atoms but also the strong repulsive forces exerted by the solid near the pore walls. In this respect the "accessible" (often reported as "chemical" or "effective") pore width, w, should be used. The accessible pore volume can be defined as the volume for which a molecule has a non-positive s–f potential. Following this definition, it can be determined by a method adopted by Do and Do (2006) which resembles a "Hit and miss" Monte Carlo volume integration as follows: an argon particle is randomly inserted into the empty pore space of the slit, and if its s–f potential energy is negative, it is registered as a "success" hit. This process is repeated many times (10^7 in our case), the percentage of "success" hits is calculated and this is taken to be the ratio of the accessible over the physical pore volume. The relationship between the physical and the accessible pore size is depicted in Fig. 2, where literature data from Liu et al. (2012) have also been included. As expected, the accessible pore size depends on the surface oxygen content, since the protruding functionalities make the slit pore statistically narrower.

3 Results and discussion

3.1 Surface heterogeneity

In order to study the potential field heterogeneity of the functionalized surfaces, a gridding technique was used

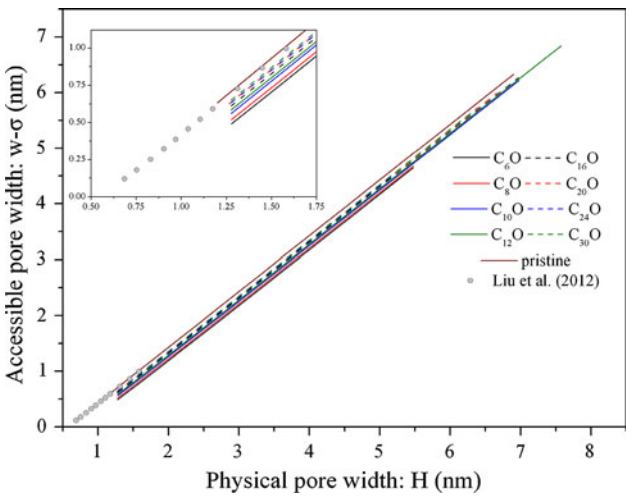

Fig. 2 The accessible pore size for argon versus physical pore size for slit pores with oxygen functionalized surfaces

(Vishnyakov et al. 1998). In detail, the surfaces were divided into 80 × 80 rectangular meshes, resulting in 6,400 (x, y) nodes (Δx and Δy intervals appr. 0.03 nm). The z direction (perpendicular to the surface) was further divided to "slices" up to z = 1.5 nm away from the surface, with intervals of 0.01 nm. We computed fluid–solid interactions for each (x, y) node and over all z intervals producing thus 6,400 U(z) interaction profiles. For each U(z) profile we stored the strongest fluid–solid interaction (i.e., local interaction energy minimum, $U_{min}(x, y)$) along with its location (i.e., distance from the surface z_{min}). It should be noted that periodic boundary conditions were used to avoid additional finite length induced heterogeneities. Following this approach, surface heterogeneity can be highlighted by "minimum energy" and "minimum energy distance" maps as the ones presented in Fig. 3 (referring to the $C_{16}O$ surface). The interaction is rather enhanced in the vicinity of oxygen groups, while on top of them $U_{min}(x, y)$ is located at an increased distance z from the graphitic surface. This is expected as the oxygen atoms repulse fluid molecules preventing them to approach too close to the carbon surface. Actually, due to the C–O–H bonding, differences in the location of minimum interaction energy are more evident for hydroxyl than for epoxy groups. Enhancement of energy is expected at the surrounding sites of the oxygen groups where interactions stemming form nearest carbon, oxygen and/or hydrogen atoms overlap. The hexagonal pattern along the non functionalized regions of the surface depicts the honeycomb lattice of carbon atoms as the interaction potential is greater at the centre than on the edges of carbon rings.

In Fig. 4 the statistical distributions of local interaction energy minimum values and distances (U_{min} values and z_{min}) are presented for all the models tested. The functionalised surfaces are compared with a completely homogeneous (pristine) structure. The pristine case is defined either as a purely structureless model (Eq. 2) or as a shifted (by Δ = 0.335 nm) structureless model furnished on top with an atomistically described graphene layer (Fig. 1b). Both definitions are statistically identical as they reveal peaks at the same U_{min} and z_{min} values: $(U_{min}/\varepsilon, z_{min}/\sigma) = (-8.943, 1.007)$; however as expected the purely structureless model reveals a delta type distribution in contrast to the Gaussian atomistic one, in which the fine structure of the benzene rings' local heterogeneity is revealed. On the other hand the energetic distribution of the adsorption sites along the oxidised surfaces highlights their heterogeneity as the energy variance is rapidly increasing with increased surface functionalization leading also to a wide spatial distribution of local interaction maxima. In fact the U_{min} distributions over the functionalised surfaces consist of two peaks. The first one is shifted towards

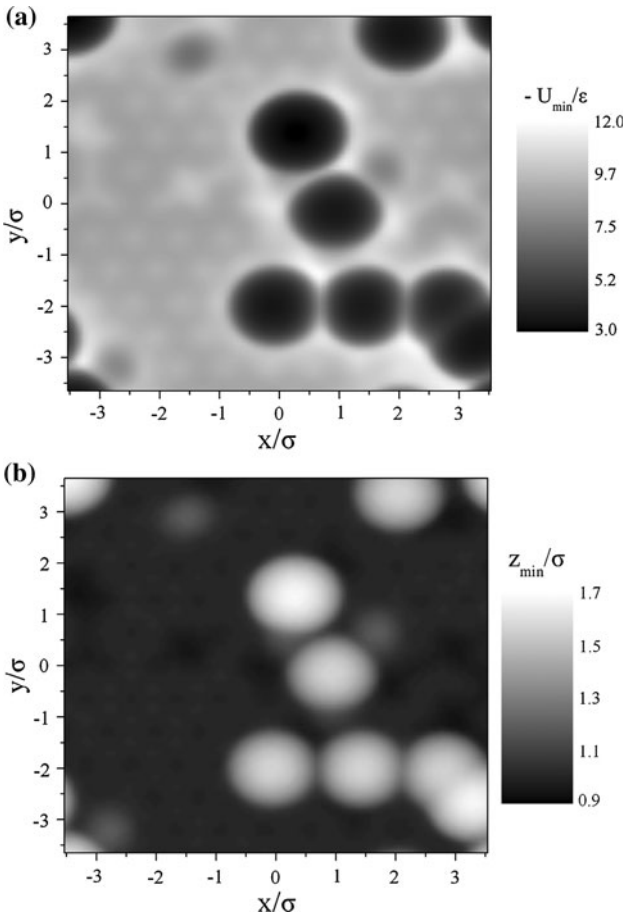

Fig. 3 Map of **a** the local minimum energy (maximum interaction), U_{min} and **b** the distance from a fluid molecule to the oxidized graphitic surface z_{min} at which $U = U_{min}$ for the model $C_{16}O$

stronger interactions (compared to pristine), because a molecule located between oxygen groups is in general closer to more sites and thus obtains a more negative U_{min}. The second weaker interaction peak ($-6 < U_{min}/\varepsilon < -2$) refers to the area above the oxygen groups and is located away from the carbon surface (>1.6 molecular diameters). It is noteworthy that for surfaces with densely packed oxygen groups (e.g., C_6O or C_8O) the spatial distribution of minimum energies (maximum interactions) is quite flat inside the range of the aforementioned energy values and this is expected to lead to highly delocalized adsorbed layers. In all cases the underlying feature of these distributions is that as the oxygen content increases, patches with considerably different energies are developed rendering the energy and the position of an admolecule not fixed and resulting in less localised adsorption equilibria compared to an homogeneous (pristine) surface, in accordance with the theory of adsorption on heterogeneous surfaces (Jaroniec and Madey 1988; Bakaev and Steele 1992).

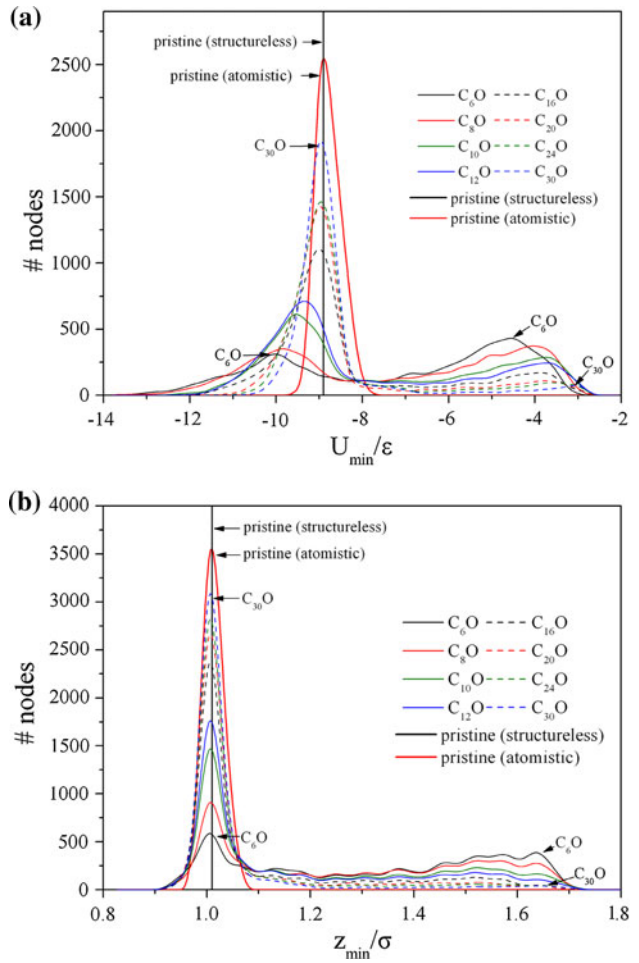

Fig. 4 Adsorption site distribution on oxygen functionalized surfaces with different C:O ratios. Energies (**a**) and positions (**b**) correspond to minimal energy $U_{min}(x, y)$ (i.e., maximum interaction) and the position from the surface where $U = U_{min}$

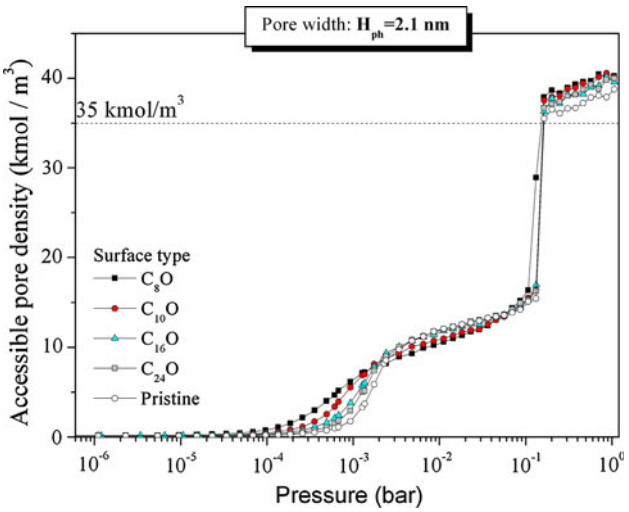

Fig. 5 Simulated isotherms of argon adsorption in slit pores with different surface content of oxygen functionalities at 87 K. The physical width of all slit pores is H = 2.1 nm (densities refer to the accessible pore volume)

3.2 Adsorption dependence on the surface oxygen content

An indicative set of argon adsorption isotherms at 87 K for slit pores having the same size (H = 2.1 nm) but different surface oxygen content is presented in Fig. 5 (as density vs. pressure) along with the non-functionalized (pristine) pore. The densities have been calculated on the basis of accessible pore volume and it should be noted that although the "physical" volumes of all the pores are identical (as the "physical" dimensions are the same), the accessible pore volumes differ for different oxygen concentrations.

All isotherms qualitatively reveal the same features, i.e., initial density increase associated with the development of a monolayer, smooth multilayer formation, a sudden density transition as argon condenses in the pores and a further liquid densification at high pressures. A straightforward observation is that surface heterogeneity does not significantly affect the condensation pressure (>0.1 bar); a slight difference is only observed for the very high surface oxygen concentration of C_8O. This is logical since condensation occurs at the pore core where the s–f interaction is weak and thus surface chemistry is not expected to have a critical role. On the other hand, at low coverage, during the first layer formation ($p < 0.003$ bar), the effect of functionalization is obvious. The isotherm of the oxygen-free pore reveals a clear layering transition, while by increasing the surface oxygen content, this transition gradually smoothens-out. This is a direct effect of heterogeneity as described in Sect. 3.1. In detail the variance of the s–f interaction energy is increasing with increased surface functionalization. Thus adsorption sites of varying energy are created on the surface and these sites are filled gradually with increasing chemical potential (pressure). On the other hand s–f interactions all over the pristine surface are rather constant thus a sharp transition is expected. Beyond monolayer formation, it can be observed that as the oxygen concentration increases the density of the adsorbed layer(s) decreases. However differences are minimized with increasing pressure and the density of the adsorbed phase just before the condensation transition are almost identical for all the structures. This can be explained based on the fact that beyond the monolayer, adsorbed molecules do not "feel" the subtleties of the surface atomic structure as the s–f interaction becomes weaker and f–f interactions start to prevail (Bakaev and Steele 1992). At higher pressures, after the condensation transition there is a further densification of the adsorbed phase reaching densities slightly above the bulk liquid density of argon (35.5 kmol/m^3). It could also be argued that the density of the adsorbed

phase when the pores are filled is increasing with increasing oxygen content (presumably due to the overall enhanced interaction), however the differences may be considered within the errors of the GCMC calculations (originating from low insertion-deletion acceptance rates when the pores are filled).

The isosteric heat versus loading for the same set of pores is presented in Fig. 6a. As expected due to the enhanced fluid-wall interactions, at zero loading the enthalpy values increase with surface oxygen content (Liu et al. 2011). The isosteric heat is maximized at the completion of the first layer, where almost the same enthalpy values for all adsorption systems have been calculated (appr. 12 kJ/mol). As in the isotherms of Fig. 5 it can again be observed that layering is smoother and shifted to lower coverage with increasing oxygen content. Thus although interactions are stronger, the monolayer is less dense in functionalized pores due to inefficient molecular packing (or else delocalized layering). A more detailed picture can be obtained by "splitting" the enthalpy contributions to s–f and f–f components (Fig. 6b). Although the f–f curves are as expected identical, the s–f curves of the "heterogeneous" pores initially decrease with loading since there is a distribution of surface energies and fluid particles cover adsorption sites in a high-to-low energy fashion (Yang and Yue 2007). On the contrary the homogeneous (pristine) pore reveals a constant s–f curve (all adsorption sites are of equal energy). Monolayer completion is coupled with a sudden drop of the s–f contribution and it can again be clearly seen that heterogeneous pores form monolayers at lower coverage. On the other hand as coverage increases the f–f contributions increase also. And this actually occurs in a way that for all the pores studied the sum of s–f and f–f remains constant (12 kJ/mol) at monolayer completion.

The structure of the adsorbed phase inside the pores can be studied on the basis of pore density profiles for various equilibrium pressures. Figure 7a and b present the density profiles during monolayer formation. Initially, before the monolayer is formed, the density is highest for the pore with the most oxidized surface. However upon monolayer completion, the pristine pore obtains the highest density due to the more efficient molecular packing over smooth surfaces. Moreover in slightly greater pressures (Fig. 7c) it can be seen that because of the irregular packing, inside the most heterogeneous pore a second layer is being formed, while the monolayer has not been fully densified (compared to the pristine pore). Figure 7d depicts a high equilibrium pressure where the pores have been filled. It is evident that the adsorbed layers of the pristine pore are more localized and dense compared to the pores with surface functionalities, because wall heterogeneities destabilize the adsorbed phase making the particles more uniformly distributed over the whole width of the pore. Additionally, as the oxygen content is increased formation of sub-layers is observed. This sub-layered structure is a direct effect of the oxygen functionalities that are placed in standard distance from the surface giving rise on the average to an "extra" oxygen rich surface inside the pore. The structure of the monolayer for each surface type (up to 1.7 molecular diameters from the slit walls) is highly correlated with the spatial distribution (z_{min}) of the respective open surfaces of Fig. 4b.

3.3 Adsorption dependence on the pore size

In Fig. 8 an example of MC calculated argon adsorption isotherms at 87 K for slit pores of varying physical width, H, having the same surface oxygen concentration ($C_{10}O$) is

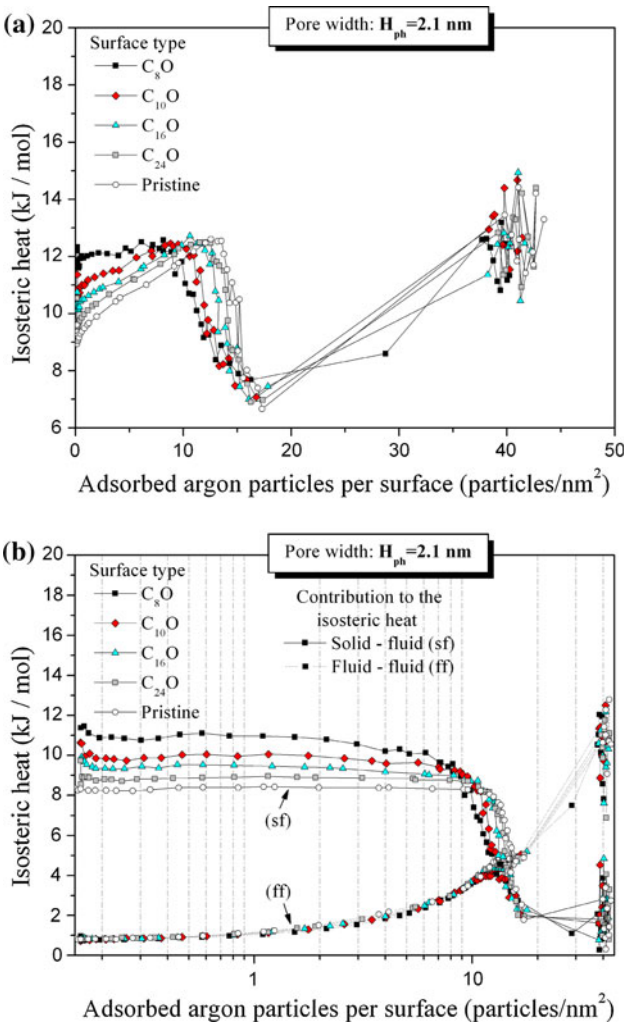

Fig. 6 **a** Isosteric heats of argon adsorption in slit pores of H = 2.1 nm physical width having different surface oxygen concentrations. Loading is expressed as adsorbed argon particles per unit surface of the pore. **b** Solid–fluid and fluid–fluid potential contribution to the isosteric heat of argon adsorption in slit pores with different content of oxygen functional groups

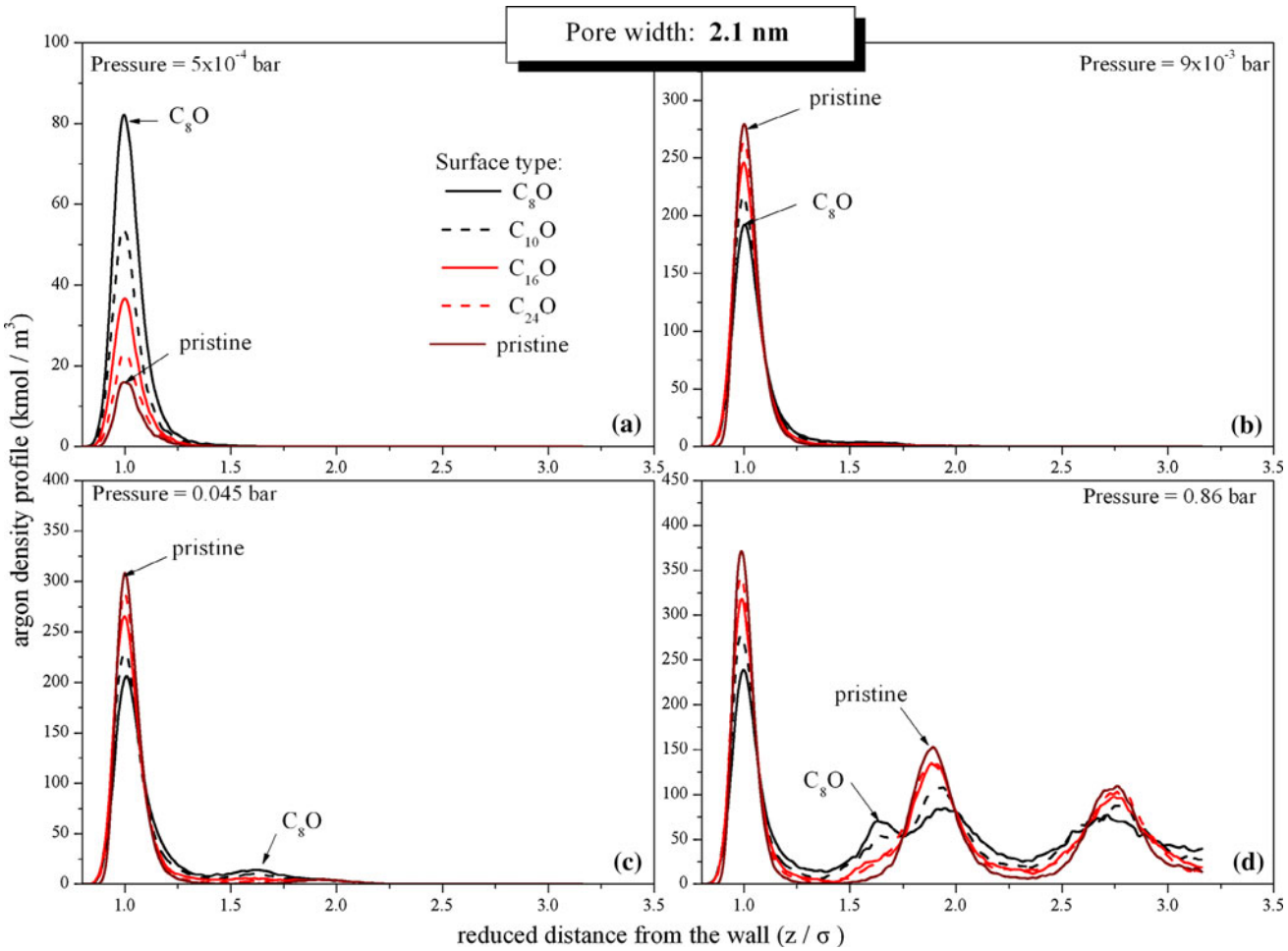

Fig. 7 Density distributions of argon particles adsorbed in slit pores (H = 2.1 nm) with different content of oxygen functionalities on their surface, along the distance from the surface for different equilibrium pressures

presented. Again the adsorbed density has been calculated on the basis of the accessible (chemical or effective) pore volume. For the smaller pore size presented (H = 1.2 nm) a continuous curve pointing to micropore filling is observed. For wider pores a sharp density change denoting capillary condensation is revealed. As expected, condensation is shifted to higher pressures as the pore width increases. Further density increase after the condensation transition is due to the compression of the liquid condensate, while the calculated densities are slightly larger than that of bulk liquid Ar at 87 K (35.5 kmol/m^3).

During the initial steps of adsorption (low pressure region) the number of the adsorbed particles depends on s–f interactions and therefore on the surface chemistry of the walls. In this respect, for adequately wide pores, the molecular packing during the monolayer formation should be unaffected by the size of the pore provided that the surface chemistry is the same. This is shown in Fig. 8b where adsorption is expressed as adsorbed particles per unit surface of the adsorbent and also in Fig. 9a where the isosteric heat of adsorption versus loading is presented for the same set of slit pores. Both the isotherms and the isosteric curves for all the pores, except the H = 1.2 nm slit, coincide up to the pressure or coverage threshold where condensation occurs. The enhancement of adsorption in the narrowest pore is a pure confinement effect (micropore filling) and is attributed to the additive interactions of opposing pore walls as the pore width is comparable to the diameter of the fluid molecules. For the same reason, for the smallest pore there is no clear distinction of a first to second layer transition and the isosteric heat increases linearly with coverage until the (micro) pore is completely filled. Larger pores, reveal almost identical layering transitions since at low pressures adsorption is determined mainly by the wall-fluid interactions. Of course the pore width determines the condensation pressure as well as the total number of argon particles adsorbed (before and after condensation). During monolayer formation, the isosteric heat increases with loading due to f–f interactions while the heat attributed to

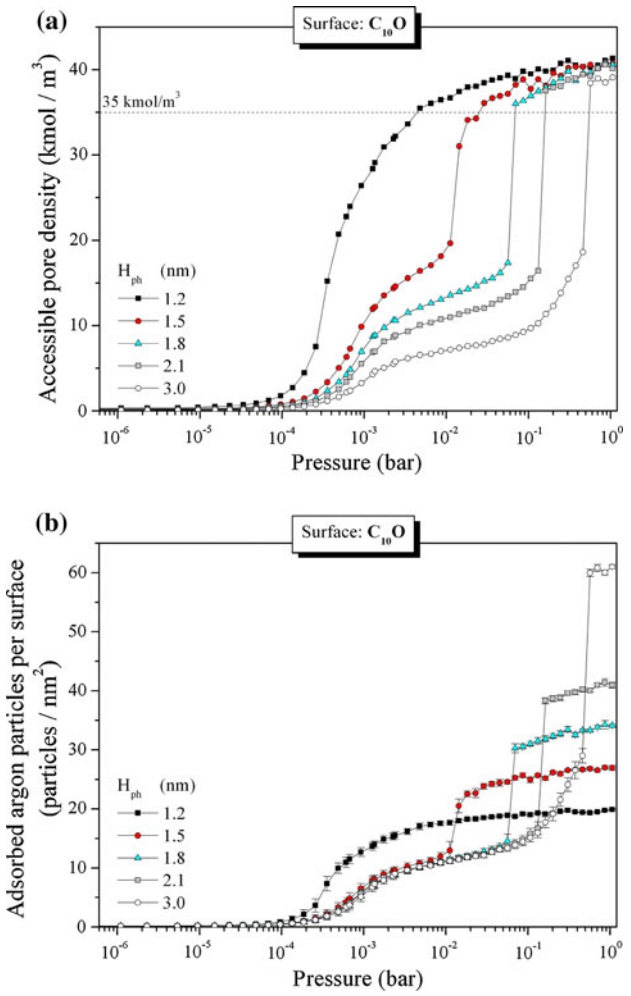

Fig. 8 Simulated isotherms of argon adsorption in slit pores of different size with $C_{10}O$ surface chemistry at 87 K expressed as **a** densities and **b** particles per surface area

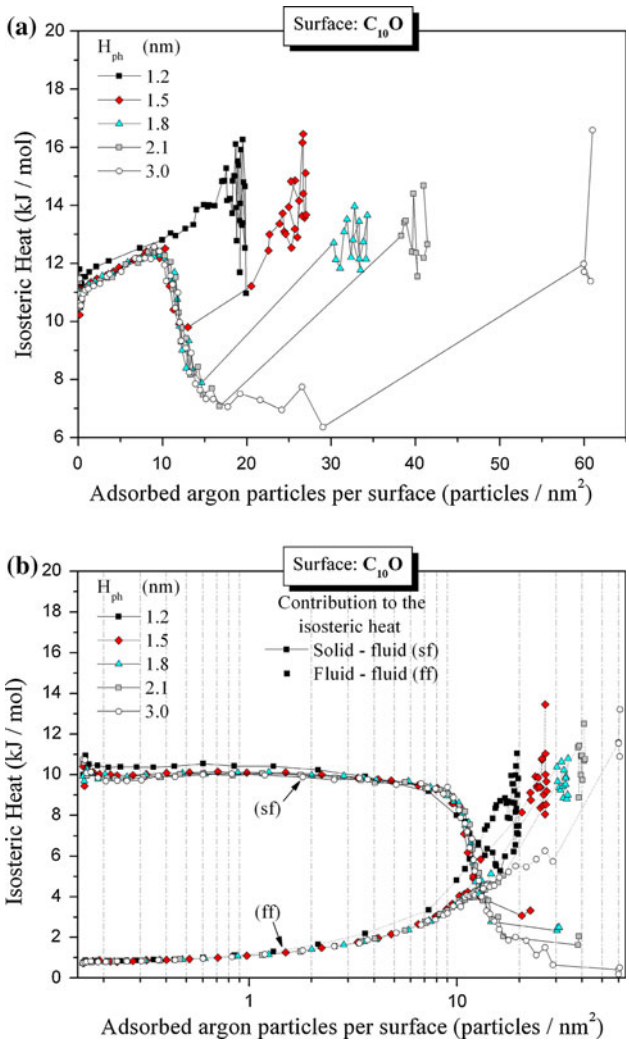

Fig. 9 **a** Isosteric heats of argon adsorption for a set of $C_{10}O$ slit pores **b** solid–fluid and fluid–fluid potential contribution to the isosteric heat of argon adsorption

the s–f interactions decreases (Fig. 9b). The negative slope of the s–f contribution on the energy in Fig. 9b, is characteristic of adsorption on heterogeneous surfaces because adsorption starts from the highly attractive surface sites and proceeds to the weaker ones. The peak of the isosteric heat corresponds to the completion of monolayer; thereafter the isosteric heat drops exponentially due to the reduced interaction of the subsequent layer(s) with the pore wall. At higher loadings, argon condenses inside the H = 1.5 (4.5σ), 1.8 (5.4σ), and 2.1 nm (6.3σ) pores at successively greater values of coverage, (Figs. 8a, 9a). Inside the H = 3.0 nm (9.0σ) slit a second adsorption layer formation can be detected. As can be seen in Fig. 9b the heat contributed by the s–f interaction after condensation in the H = 3.0 nm is practically zero, while for the other pores the contribution is small yet not insignificant.

3.4 Pore filling pressure

The adsorption isotherms of three pore sizes having the eight cases of surface heterogeneity considered are presented in Fig. 10. It is clear that for small pore sizes (Fig. 10a) oxygen functionalities strongly influence the micropore filling process because all the adsorbed molecules interact strongly with the surface oxygen groups due to confinement. For wider pores (Fig. 10b), surface heterogeneity actually affects only the layering transition(s) as the molecules that are located in the core of the pore are practically unaffected by the surface chemistry (being away from the pore walls). In this respect surface functionalities may seem to have an effect on condensation pressure but this is only due to the statistical pore "narrowing" that is imposed. For even larger pores (Fig. 10c) even this narrowing seems to be insignificant and the

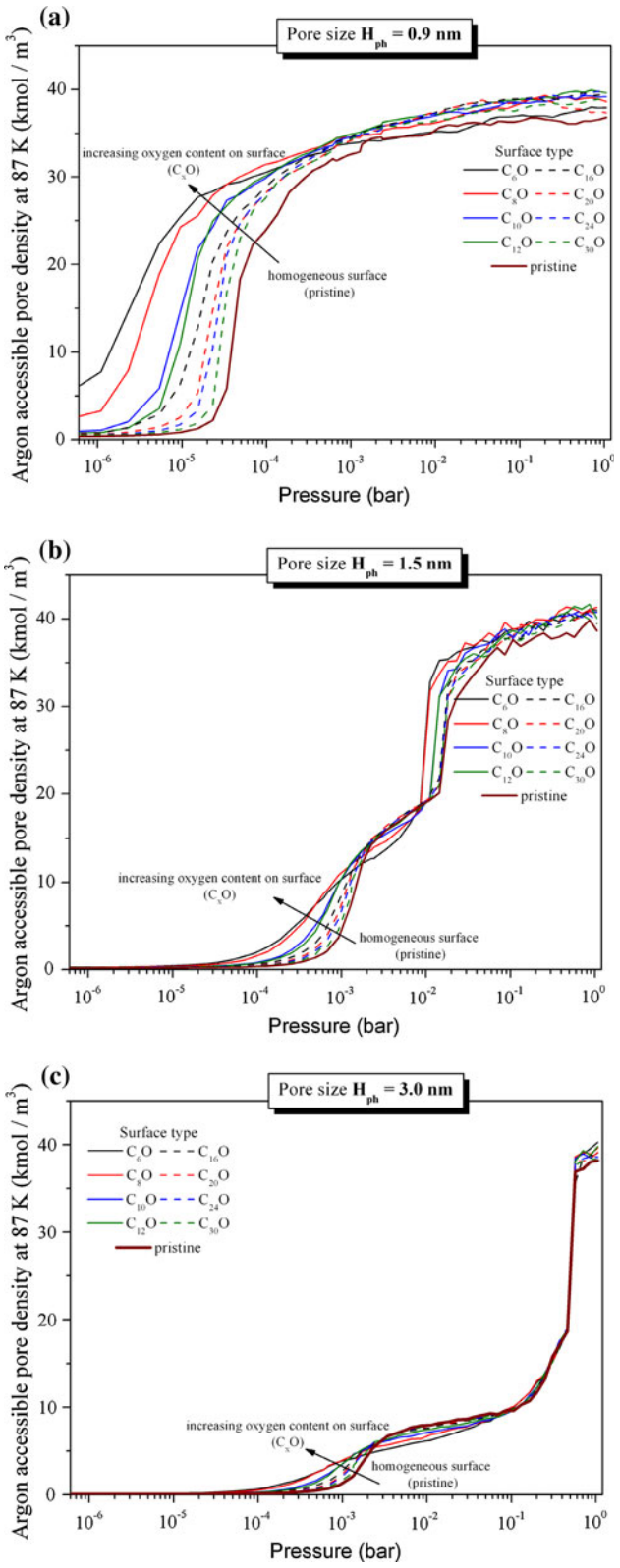

Fig. 10 Comparison of the argon adsorption isotherms at 87 K as the oxygen content on the slit walls increases. Pore sizes **a** 0.9 nm, **b** 1.5 nm, and **c** 3.0 nm

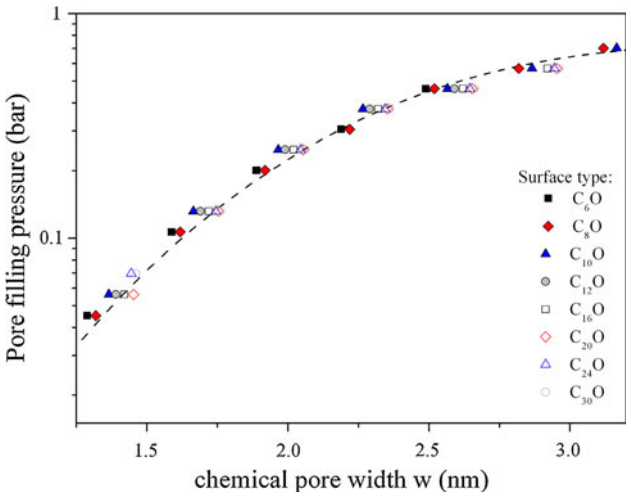

Fig. 11 Argon pore filling pressure in respect with the pore size for a set of slit pores with different oxygen surface content

condensation transition occurs at the same pressure for all the pores. In general condensation is found to depend mainly on the "accessible" pore size and not the surface chemistry. This is depicted in Fig. 11, where the pore filling pressures for pores that reveal condensation transitions have been plotted as a function of the "effective" (chemical) pore size. Our simulations were performed at the same sequence of equilibrium pressures for all cases. The pressure steps on this sequence are relatively few at the high pressure range giving a limited pressure resolution. As a result, there are "groups" of points with slightly different pore size but the same filling pressure. Nevertheless, it is quite obvious that all the different surface chemistry models degenerate into practically one "capillary condensation" curve. Based on the above, a major conclusion of this work is that argon isotherms are an excellent tool for determining mesopore size distributions, as argon is adequately inert and its condensation in capillaries remains unaffected of surface functionalities (and thus any other kind of geometrical or energetic heterogeneity) (Dombrowski et al. 2000; Kruk and Jaroniec 2000). On the other hand even a molecule as inert as argon has a significantly different behavior in energetically "heterogeneous" micropores. Therefore micropore size distributions based on argon isotherms, should definitely take into account the surface chemistry of the material studied. It should finally be mentioned that the effects of surface chemistry are expected to be much more enhanced for N_2 or CO_2 that possess quadrupole moments and are expected to have strong Coulombic interactions with the surface groups (Furmaniak et al. 2009, 2010). For these cases significant effects are expected even in the mesopores range. Our group is currently working on this issue.

4 Conclusions

The effect of functionalization on the adsorption characteristics of Ar at 87 K has been studied by GCMC inside individual pores of varying size and surface oxygen concentration. It is concluded that the insertion of oxygen functionalities in small micropores has a significant qualitative and quantitative effect in argon adsorption. Functionalized micropores are filled in much lower pressures since all the adsorbed molecules interact strongly with the surface oxygen groups due to confinement. Similarly in larger pores there are profound differences in the adsorbed monolayer as well as in the structure of the adsorbed phase. In detail oxygen functionalization smoothes out layering transitions while the functionalities cause severe delocalization of adsorbed molecules and thus less defined adsorbed layers. On the other hand, condensation transitions are not substantially affected by the presence of functionalities and the condensation pressure is dictated by the "effective" pore size rather than the surface chemistry. This is attributed to the fact that condensation occurs at the pore core where the s–f interaction is weak and thus surface chemistry is not expected to have a critical role. Based on the above, we may conclude that mesopores size analysis with argon isotherms at 87 K can be trustworthy even for heavily oxidized carbons, while adequate micropore (and most significantly ultra micropore) analysis requires consideration of surface chemistry issues.

References

Ahlrichs, R., Bar, M., Haser, M., Horn, H., Kolmel, J.: Electronic structure calculations on workstation computers: the program system turbomole. Chem. Phys. Lett. **162**, 165–169 (1989)

Allen, M.P., Tildesley, D.J.: Computer Simulations of Liquids. Clarendon, Oxford (1987)

Bakaev, V.A., Steele, W.A.: Grand canonical ensemble computer simulation of adsorption of argon on a heterogeneous surface. Langmuir **8**, 148–154 (1992)

Bhatia, S.K.: Density functional theory analysis of the influence of pore wall heterogeneity on adsorption in carbons. Langmuir **18**, 6845–6856 (2002)

Coasne, B., Hung, F.R., Roland, J., Pellenq, M., Siperstein, F.R., Gubbins, K.E.: Adsorption of simple gases in MCM-41 materials: the role of surface roughness. Langmuir **22**, 194–202 (2006)

Do, D.D., Do, H.D.: Modeling of adsorption on nongraphitized carbon surface: GCMC simulation studies and comparison with experimental data. J. Phys. Chem. B **110**, 17531–17538 (2006)

Dombrowski, R.J., Hyduke, D.R., Lastoskie, C.M.: Pore size analysis of activated carbons from argon and nitrogen porosimetry using density functional theory. Langmuir **16**, 5041–5050 (2000)

Furmaniak, S., Terzyk, A.P., Gauden, P.A., Harris, P.J.F., Kowalczyk, P.: Can carbon surface oxidation shift the pore size distribution curve calculated from Ar, N_2 and CO_2 adsorption isotherms? Simulation results for a realistic carbon model. J. Phys. Condens. Matter **21**, 315005–315016 (2009)

Furmaniak, S., Terzyk, A.P., Gauden, P.A., Harris, P.J.F., Kowalczyk, P.: The influence of carbon surface oxygen groups on Dubinin–Astakhov equation parameters calculated from CO_2 adsorption isotherm. J. Phys. Condens. Matter **22**, 085003–085014 (2010)

Gor, G.Y., Thommes, M., Cychosz, K.A., Neimark, A.V.: Quenched solid density functional theory method for characterization of mesoporous carbons by nitrogen adsorption. Carbon **50**, 1583–1590 (2012)

Gotzias, A., Tylianakis, E., Froudakis, G., Steriotis, Th: Theoretical study of hydrogen adsorption in oxygen functionalized slit pores. Microporous Mesoporous Mater. **154**, 38–44 (2012)

Haenel, M.W.: Recent progress in coal structure research. Fuel **71**, 1211–1223 (1992)

Jagiello, J., Olivier, J.: A simple two-dimensional NLDFT model of gas adsorption in finite carbon pores. Application to pore structure analysis. J. Phys. Chem. C **113**, 19382–19385 (2009)

Jaroniec, M., Madey, R.: Physical Adsorption on Heterogeneous Solids. Elsevier, Amsterdam (1988)

Kruk, M., Jaroniec, M.: Accurate method for calculating mesopore size distributions from argon adsorption data at 87 K developed using model MCM-41 materials. Chem. Mater. **12**, 222–230 (2000)

Kuchta, B., Firlej, L., Boulet, P., Marzec, M.: Adsorption in cylindrical pores: mixed lattice-site/off-site Monte Carlo simulations in pores with heterogeneous wall structure. Appl. Surf. Sci. **253**, 5596–5600 (2007)

Lee, S.Y., Park, S.J.: Influence of oxygen-functional groups on carbon replicas for hydrogen adsorption. Phys. Status Solids A **209**, 694–697 (2012)

Liu, Y., Wilcox, J.: Molecular simulation of CO_2 adsorption in micro- and mesoporous carbons with surface heterogeneity. Int. J. Coal Geol. **104**, 83–95 (2012)

Liu, Z., Do, D.D., Nicholson, D.: Effects of confinement on the molar enthalpy of argon adsorption in graphitic cylindrical pores: a grand canonical Monte Carlo (GCMC) simulation study. J. Colloid Interface Sci. **361**, 278–287 (2011)

Liu, Z., Horikawa, T., Do, D.D., Nicholson, D.: Packing effects on argon and methanol adsorption inside graphitic cylindrical and slit pores: a GCMC simulation study. J. Colloid Interface Sci. **368**, 474–487 (2012)

Maddox, M.W., Olivier, J.P., Gubbins, K.E.: Characterisation of MCM-42 using molecular simulation: heterogeneity effects. Langmuir **13**, 1737–1745 (1997)

Marsh, H., Rodriguez-Reinoso, F.: Activated Carbon. Elsevier, London (2006)

Miyasaka, K., Neimark, A.V., Terasaki, O.: Density functional theory of in situ synchrotron powder X-ray diffraction on mesoporous crystals: argon adsorption on MCM-41. Phys. Chem. C **113**, 791–794 (2009)

Monson, P.: Understanding adsorption/desorption hysteresis for fluids in mesoporous materials using simple molecular models and classical density functional theory. Microporous Mesoporous Mater. **160**, 47–66 (2012)

Neimark, A.V., Lin, Y., Ravikovitch, P.I., Thommes, M.: Quenched solid density functional theory and pore size analysis of micro–mesoporous carbons. Carbon **47**, 1617–1628 (2009)

Neimark, A., Ravikovitch, P., Grun, M., Schuth, F., Unger, K.: Pore size analysis of MCM-41 type adsorbents by means of nitrogen and argon adsorption. J. Colloid Interface Sci. **207**, 159–169 (1998)

Palmer, J.C., Gubbins, K.E.: Atomistic models for disordered nanoporous carbons using reactive force field. Microporous Mesoporous Mater. **154**, 24–37 (2012)

Pellenq, R.J.M., Levitz, P.E.: Capillary condensation in disordered mesoporous medium: a grand canonical Monte Carlo study. Mol. Phys. **100**, 2059–2077 (2002)

Puibasset, J.: Grand canonical, Helmoltz free energy and entropy calculation in heterogeneous cylindrical pores by the grand canonical Monte Carlo simulation method. J. Phys. Chem. B **109**, 480–487 (2005)

Ravikovitch, P.I., Jagiello, J., Tolles, D., Neimark, A.V.: Improved DFT methods for micropore size characterisation of activated carbons: role of pore wall heterogeneity. In: Extended Abstracts Carbon '01, Lexington (2001)

Rowley, L.A., Nicholson, D., Parsonage, N.G.: Grand ensemble Monte Carlo studies of physical adsorption. Mol. Phys. **31**, 365–387 (1976)

Silvestre-Albero, J., Silvestre-Albero, A., Rodriguez-Reinoso, F., Thommes, M.: Physical characterization of activated carbons with narrow microporosity by nitrogen (77.4 K), carbon dioxide (273 K) and argon (87.3 K) adsorption in combination with immersion calorimetry. Carbon **50**, 3128–3133 (2012)

Smith, K.L., Smoot, L.D., Fletcher, T.H., Pugmire, R.J.: The Structure and Reaction Processes of Coal. Plenum Press, New York (1994)

Steele, W.A.: The physical interaction of gases with crystalline solids. Surf. Sci. **36**, 317–352 (1973)

Steele, W.A.: The Interaction of Gases with Solid Surfaces. Pergamon Press, Oxford (1974)

Tenney, C.M., Lastoskie, C.M.: Molecular simulation of carbon dioxide adsorption in chemically and structurally heterogeneous porous carbons. Environ. Prog. **25**, 343–354 (2006)

Tjatjopoulos, G.J., Feke, D.L., Mann, J.A.: Molecule micropore interaction potentials. J. Phys. Chem. **92**, 4006–4007 (1998)

van Krevelen, D.W.: Coal, 3rd edn. Elsevier, Amsterdam (1991)

Vishnyakov, A., Piotrovskaya, E.M., Brodskaya, E.N.: Capillary condensation and melting/freezing transitions for methane in slit coal pores. Adsorption **4**, 207–224 (1998)

Wang, Y., Do, D.D., Nicholson, D.: Study of heat of adsorption across the capillary condensation in cylindrical pores. Colloids Surf. A Physicochem. Eng. Asp. **380**, 66–78 (2011)

Wang, Z., Yang, F.H., Yang, R.T.: Enhanced hydrogen spillover on carbon surfaces modified by oxygen plasma. J. Phys. Chem. C **114**, 1601–1609 (2010)

White, C.M., Smith, D.H., Jones, K.L., Goodman, A.L., Jikich, S.A., LaCount, R.B., DuBose, S.B., Ozdemir, E., Morsi, B.I., Schroeder, K.T.: Sequestration of carbon dioxide in coal with enhanced coalbed methane recovery—a review. Energy Fuels **19**, 659–724 (2005)

Wisniewski, M., Furmaniak, S., Kowalczyk, P., Werengowska, K.M., Rychlicki, G.: Thermodynamics of benzene adsorption on oxidized carbon nanotubes—experimental and simulation studies. Chem. Phys. Lett. **538**, 93–98 (2012)

Yang, X., Yue, X.: Adsorption of structure Lennard-Jones model fluid in slit-like amorphous silica nanopores. Colloids Surf. A Physicochem. Eng. Asp. **301**, 166–173 (2007)